Comparison of Hydrodynamics and Mass Transfer in Airlift and Bubble Column Reactors Using CFD

By *J. M. van Baten* and *R. Krishna**

Computational Fluid Dynamics (CFD) is used to compare the hydrodynamics and mass transfer of an internal airlift reactor with that of a bubble column reactor, operating with an air/water system in the homogeneous bubble flow regime. The liquid circulation velocities are significantly higher in the airlift configuration than in bubble columns, leading to significantly lower gas holdups. Within the riser of the airlift, the gas and liquid phases are virtually in plug flow, whereas in bubble columns the gas and liquid phases follow parabolic velocity distributions. When compared at the same superficial gas velocity, the volumetric mass transfer coefficient, k_La, for an airlift is significantly lower than that for a bubble column. However, when the results are compared at the same values of gas holdup, the values of k_La are practically identical.

1 Introduction

Bubble columns are widely used in industry for carrying out a variety of chemical reactions such as hydrogenations, chlorinations, oxidations, and the Fischer Tropsch synthesis [1]. In bubble column slurry reactors, catalyst particle sizes smaller than about 100 μm can be used, thus eliminating intra-particle diffusion resistances. These catalyst particles are held in suspension due to liquid circulation caused by the rising gas bubbles. When the skeletal density of the catalyst is high there is a danger of catalyst settling in the bubble column reactor; this possibility arises, for example, in the hydrogenation of nitriles using Raney catalyst [2,3]. The introduction of a draft tube into the bubble column reactor causes a substantial increase in the liquid circulation, for the same gas flow, and helps to keep the particles in suspension. A bubble column with an internal draft tube is also termed an internal airlift reactor, Fig. 1.

The gas sparger is located in the riser, and the other part is the downcomer. The driving force, based on the static pressure difference, or the mixture density difference, between the riser and the downcomer generates the liquid circulation in a loop. Airlift reactors are finding increasing applications in the chemical industry, biochemical fermentation, and biological wastewater treatment processes [4–6]. Compared with conventional reactors, such as stirred tank reactors or bubble columns, shear stress is relatively constant and mild throughout the reactor.

For design of an airlift reactor, it is necessary to have accurate estimates of the phase holdups and velocities in the riser and downcomer. Several literature studies have focused on the estimation of these hydrodynamic parameters [7–9]. In particular, the velocities of the liquid in the downcomer and riser are crucially dependent on the frictional losses, which in turn are determined by the geometry of the reactor and the operating conditions. Several empirical correlations have been proposed for the estimation of these hydrodynamic parameters; however, these correlations are restricted in their applicability to the geometry for which they were determined. Extrapolation to other geometries, scales, and operating conditions is fraught with uncertainty. While there are a few experimental studies, which have focused on the interphase mass transfer in airlift reactors [10–12], there appear to be no generally applicable models or correlations for the estimation of the volumetric mass transfer coefficient, k_La, in airlift reactors.

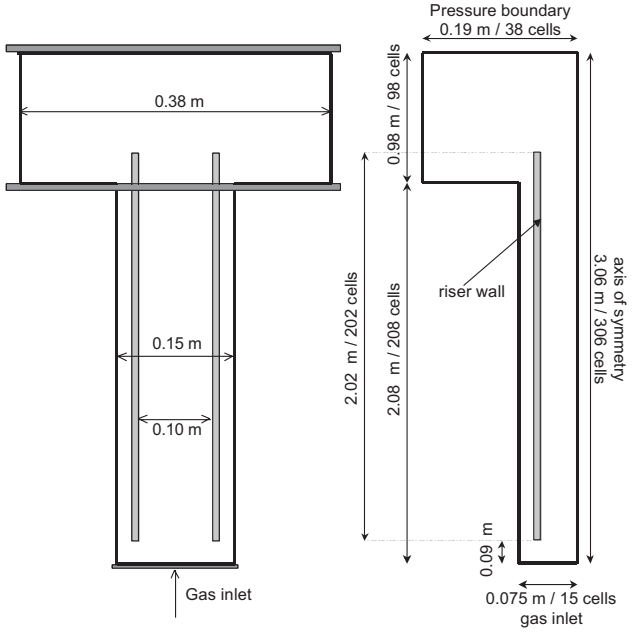

Figure 1. Schematic of airlift reactor, showing the computational domains and grid details.

Several recent publications have established the potential of Computational Fluid Dynamics (CFD) for describing the *hydrodynamics* of bubble columns [13–18]. An important advantage of the CFD approach is that column geometry and scale effects are automatically accounted for. The first major objective of the present communication is to develop a CFD model for internal airlift reactors to describe not only the

[*] J. M. van Baten, R. Krishna (author to whom correspondence should be addressed, e-mail: krishna@science.uva.nl), Department of Chemical Engineering, University of Amsterdam, Nieuwe Achtergracht 166, 1018 WV Amsterdam, The Netherlands.

  DOI: 10.1002/ceat.200301796

hydrodynamics but also *interphase mass transfer*. The second objective is to compare the mass transfer performance of airlift and bubble column reactors in a consistent manner.

2 Development of the CFD Model

Eulerian simulations were carried out for an airlift reactor, shown schematically in Fig. 1. This geometry corresponds to an experimental setup used in our earlier study [19], consisting of a polyacrylate column with an inner diameter of 0.15 m and a length of 2 m. At the bottom of the column, the gas phase is introduced through a perforated plate with 625 holes of 0.5 mm diameter. A polyacrylate draft tube (riser) of 0.10 m inner and 0.11 m outer diameter with a height of 2.02 m is mounted into the column 0.10 m above the gas distributor. The downcomer itself is 0.02 m wide. In order to avoid gas flow into the downcomer section, a gas-liquid separator is mounted at the top of the column, 1 m in height and 0.38 m in diameter. Further details of the experimental set up can be found on the web site: http://ct-cr4.chem.uva.nl/airlift/.

The superficial gas velocity, U_G, at the bottom inlet was varied in the range 0.02–0.12 m/s. The physical and transport properties of the gas and liquid phases are specified in Tab. 1.

Table 1. Properties used in the CFD simulations.

	Liquid (water)	Gas (air)
Viscosity, μ/[Pa s]	1×10^{-3}	1.7×10^{-5}
Diffusivity of mass tracer, D/[m^2 s^{-1}]	1×10^{-9}	1.0×10^{-5}
Density, ρ/[kg/m^3]	998	1.3
Interphase mass transfer coefficient, k_L/[m/s]	0.0004	
Henry coefficient, H/[–]	0.05	
Surface tension, σ/[N/m]	0.073	

In each case two different types of simulation were carried out:

- Determination of the steady-state hydrodynamics.
- Determination of the interphase mass transfer by introducing a soluble, non-reactive, component (tracer) in the gas phase.

Firstly, the CFD modeling of the steady-state hydrodynamics is discussed.

For either fluid phase in the bubble column reactor, the volume-averaged mass and momentum conservation equations in the Eulerian framework are given by:

$$\frac{\partial\left(\varepsilon_k \rho_k\right)}{\partial t} + \nabla \cdot \left(\rho_k \varepsilon_k \boldsymbol{u}_k\right) = 0 \tag{1}$$

$$\frac{\partial\left(\rho_k \varepsilon_k u_k\right)}{\partial t} + \nabla \cdot \left(\rho_k \varepsilon_k \boldsymbol{u}_k \boldsymbol{u}_k - \mu_k \varepsilon_k \left(\nabla \boldsymbol{u}_k + \left(\nabla \boldsymbol{u}_k\right)^T\right)\right) = -\varepsilon_k \nabla p + \boldsymbol{M}_{kl} + \rho_k \varepsilon_k \boldsymbol{g} \tag{2}$$

where ρ_k, $\boldsymbol{u}_k$, ε_k, and μ_k represent, respectively, the macroscopic density, velocity, volume fraction, and viscosity of the kth phase, p is the pressure, $\boldsymbol{M}_{kl}$ is the interphase momentum exchange between phase k and phase l, and $\boldsymbol{g}$ is the gravitational acceleration[1)].

The momentum exchange between the gas (subscript G) and liquid phase (subscript L) phases is given by:

$$\boldsymbol{M}_{L,G} = \frac{3}{4} \rho_L \frac{\varepsilon_G}{d_G} C_D \left(\boldsymbol{u}_G - \boldsymbol{u}_L\right) \left|\boldsymbol{u}_G - \boldsymbol{u}_L\right| \tag{3}$$

Only the drag force contribution to $\boldsymbol{M}_{L,b}$ has been included, in keeping with the works of Sanyal *et al.* [20] and Sokolichin and Eigenberger [21]. The added mass and lift forces have been ignored in the present analysis.

The interphase drag coefficient is calculated from [22]:

$$C_D = \frac{2}{3}\sqrt{Eö} \tag{4}$$

where the Eötvös number is defined as:

$$Eö = \frac{g(\rho_L - \rho_G) d_b^2}{\sigma} \tag{5}$$

where d_b is the equivalent diameter of the bubbles. The bubble diameter is taken to be 0.005 m, a typical value for air-water systems operating in the homogeneous bubble flow regime.

For the continuous, liquid phase, the turbulent contribution to the stress tensor is evaluated by means of k-ε model, using standard single-phase parameters, $C_\mu = 0.09$, $C_{1\varepsilon} = 1.44$, $C_{2\varepsilon} = 1.92$, $\sigma_k = 1$, and $\sigma_\varepsilon = 1.3$. The applicability of the k-ε model was considered in detail by Sokolichin and Eigenberger [21]. No turbulence model is used for calculating the velocity fields inside the dispersed gas bubbles.

A commercial CFD package CFX, versions 4.2 and 4.4, of AEA Technology, Harwell, UK, was used to solve the equations of continuity and momentum. This package is a finite volume solver, using body-fitted grids. The grids are non-staggered and all variables are evaluated at the cell centers. An improved version of the Rhie-Chow algorithm [23] is used to calculate the velocity at the cell faces. The pressure-velocity coupling is obtained using the SIMPLEC algorithm [24]. For the convective terms in Eqs. (1) and (2), hybrid differencing was used. A fully implicit backward differencing scheme was used for the time integration.

All simulations were carried out using two-dimensional (2D) axis-symmetric grids. In the radius of the smaller part of the column, 15 equally spaced cells of 0.005 m are present. In the larger radius of the column, 38 equally spaced cells of 0.005 m are present. The draft tube (riser wall) starts at 0.09 m above the distributor, and ends 2.11 m above the distributor. The total number of cells is 6,844.

The gas was injected homogeneously over the complete bottom region. A pressure boundary condition was applied to the top of the column. A standard no-slip boundary condition

1) List of symbols at the end of the paper.

was applied at all walls, including the draft tube. The time stepping strategy used in all simulations was 100 steps at 5×10^{-5} s, 100 steps at 1×10^{-4} s, 100 steps at 5×10^{-4} s, 100 steps at 1×10^{-3} s, 200 steps at 3×10^{-3} s, 1400 steps at 5×10^{-3} s, and the remaining steps at 1×10^{-2} s, until steady state is obtained. Steady state is obtained when all variables remain constant. To prevent start-up problems, the system was initialized by setting the gas holdup within the riser to 10 %, and setting an initial upward velocity of 0.05 m/s in the riser, and a downward velocity, to match the mass balance, in the downcomer. Further details of the simulations are available on our web site: http://ct-cr4.chem.uva.nl/airlift/.

The steady-state results of a hydrodynamic run were used to start a dynamic mass transfer simulation in which the inflowing gas stream is "traced" with a component that is soluble in the liquid phase. The concentration of tracer in the inlet gas is maintained at unit (arbitrary units). The inflowing liquid stream does not contain any tracer component A.

The following component balance equations are solved for the mass tracer:

$$\frac{\partial}{\partial t}\varepsilon_k\rho_k C_{\alpha,k} + \nabla\cdot\left(\varepsilon_k\rho_k \mathbf{u}_k C_{\alpha,k} - Đ_{\alpha,k}\varepsilon_k\rho\nabla C_{\alpha,k}\right) = \rho_{\alpha,k}F_{\alpha,kl} \quad (6)$$

Here, $C_{\alpha,k}$ is the concentration of mass-tracer component α in phase k, $Đ_{\alpha,k}$ is the diffusion coefficient of mass tracer component α in phase k and $F_{\alpha,kl}$ is the flux of mass tracer component α between phases k and l. The flux $F_{\alpha,GL}$ for liquid phase L and gas phase G are defined as:

$$F_{\alpha,GL} = k_L a(C_{\alpha,L}He - C_{\alpha,G}) \quad (7)$$

Here, k_L is the mass transfer coefficient and He is the Henry coefficient for the mass-tracer. The mass transfer coefficient k_L was chosen as 4×10^{-4} m/s. The Henry coefficient He was chosen to be 0.05. The physical and transport properties of the tracer component are specified in Tab. 1. The interfacial area per unit volume of dispersion, a, is calculated from:

$$a = \frac{6\varepsilon_G}{d_b} \quad (8)$$

No flux of mass tracer is allowed through the walls. To ensure no flux of tracer occurs across flow boundaries with zero ingoing flow, the boundary value for the mass component concentration is set equal to the value inside the computational domain at each iteration for these boundaries.

For the 2D simulations, the hydrodynamic Eqs. (1) and (2) are no longer solved since the system has reached a true steady state; none of the hydrodynamic variables are subject to change any longer. Time steps of 0.1 s were taken, until the tracer concentrations in the system attained steady state.

The CFD simulation results for the hydrodynamics and mass transfer in the airlift reactor are compared with corresponding results obtained in conventional bubble columns of three different diameters, 0.1, 0.15, and 0.38 m (corresponding to the diameters of the riser, downcomer and that of the disengaging vessel at the top). The simulation strategy for the bubble columns is similar to that described in our earlier publication [18]; further details can also be found on our website http://ct-cr4.chem.uva.nl/regimes/.

3 Simulation Results

The steady-state radial distribution of (a) gas holdup, $\varepsilon_G(r)$, and (b) liquid velocities, $V_L(r)$, in the riser and downcomer of the airlift reactor are shown in Fig. 2, for a range of superficial gas velocities, U_G, based on the riser cross-sectional area.

It was noted that the gas and liquid phases can be considered to flow up the riser virtually in plug flow. With increasing superficial gas velocities, the liquid velocities start to assume a parabolic profile. Within the central core of the riser, the gas holdup profiles are nearly uniform for the whole range of U_G values.

The cross-sectional area averaged liquid velocities in the riser and downcomer, and gas holdup values in the riser, obtained from the airlift simulations, are compared in Fig. 3 with the experimentally determined values by Van Baten *et al.* [19], there is very good agreement between them.

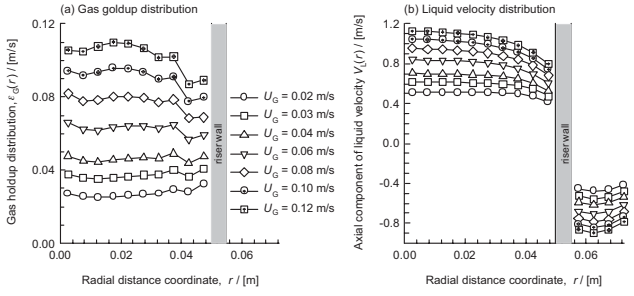

Figure 2. Radial distribution of: (a) gas holdup, $\varepsilon_G(r)$, and (b) liquid velocity, $V_L(r)$, for varying superficial gas velocities, U_G (based on cross-sectional area of riser), at a height of 1.75 m above the distributor. Animations can be viewed on the web site: http://ct-cr4.chem.uva.nl/airlift/.

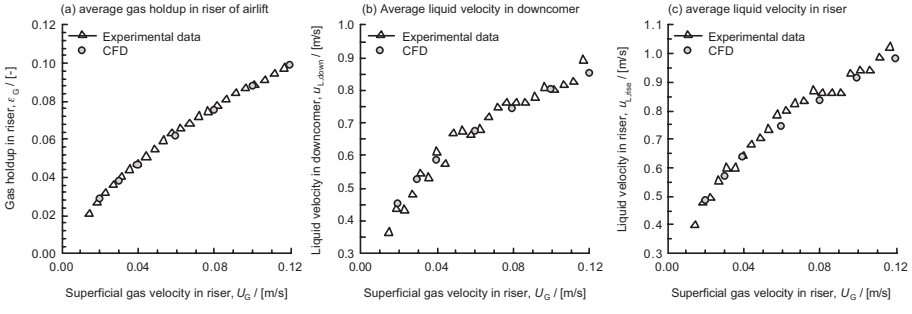

Figure 3. Comparison of airlift experimental data of van Baten *et al.* [19] with CFD simulations for gas holdup in the riser, *average* liquid velocity in the downcomer and *average* liquid velocity in the riser.

In Fig. 4 a comparison is made between the gas holdup and liquid velocity profiles in the airlift reactor operating at U_G = 0.02 m/s with the corresponding results in bubble columns of diameters 0.1 m and 0.15 m.

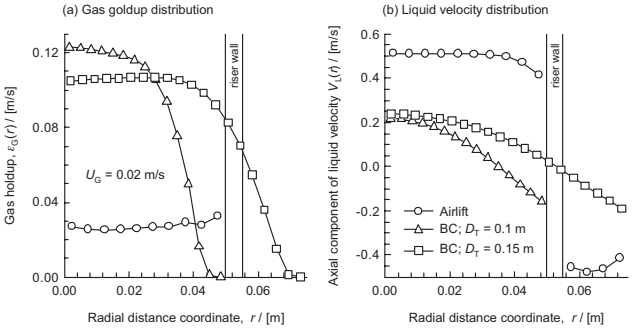

Figure 4. Radial distribution of: (a) gas holdup, $\varepsilon_G(r)$, and (b) liquid velocity, $V_L(r)$, at a height of 1.75 m above the distributor. Superficial gas U_G = 0.02 m/s (for airlift this is based on riser cross-sectional area).

The gas holdup distribution in the bubble columns has a parabolic shape and the values of $\varepsilon_G(r)$ reduce to near-zero values in the regions close to the wall of the bubble column, where the liquid velocities are reduced to negative values. The liquid velocities in the riser are considerably higher in the airlift configuration than for the bubble columns, operating at the same value of U_G. The down flowing liquid velocity in the downcomer of the airlift is also much higher than the downflow velocity in the wall regions of the bubble columns. The increased liquid circulation of the airlift, caused by the introduction of the draft tube, is a desirable feature from the point of view of catalyst suspension, for example.

The gas holdup values in Fig. 3 (a) represent the average gas fractions within the riser portion only. The gas holdup, as a fraction of the gas-liquid dispersion for the airlift system taken globally is much lower; these values are plotted in Fig. 5 (a) along with the corresponding values for bubble columns of 0.1, 0.15 and 0.38 m diameter.

The gas holdup in the airlift is significantly lower than for bubble columns, this is because of the much lower slip velocity between the gas and liquid phases within the riser of the airlift. The lower slip is due to much higher liquid circulation. The centerline liquid velocity within the riser, or bubble column, $V_L(0)$ was taken as a measure of the circulation; the values for the airlift are compared with bubble columns in Fig. 5 (b). The bubble column simulation results presented in Fig. 5 are restricted to U_G values below 0.04 m/s because for higher values of U_G the heterogeneous or churn-turbulent regime of operation is entered into [18]. The airlift reactor can be operated at U_G values up to 0.12 m/s while maintaining the homogeneous bubble flow regime since the effective slip velocity in the riser is much lower. The ability to operate in the homogeneous bubble flow region till much higher superficial gas velocities than bubble columns is a major advantage of the airlift reactors.

In published experimental studies on bubble columns [25,26], the volumetric mass transfer coefficient is usually determined by fitting the transient uptake of a soluble component (e.g., oxygen) in the liquid phase, assuming that the gas phase is in plug flow and the liquid phase is well mixed. This model leads to the following transient response for the dissolved component.

$$\frac{C_L}{C_L^*} = 1 - \exp\left(-\frac{k_L a}{1-\varepsilon_G}\, t\right) \tag{9}$$

where C_L^* is the final, steady-state, value of the liquid concentration. In order to conform with the assumptions underlying Eq. (9), the global average liquid concentration was determined (averaged over the total system liquid content of the airlift) at every time instant; a typical transience of the global concentrations is shown in Fig. 6 (a) for operation at U_G = 0.04 m/s.

The transient global concentrations are then fitted using Eq. (9) to determine the global value of k_La. For the particular run under consideration, k_La = 0.00606 s^{-1}, taking the gas holdup ε_G = 0.0156 from Fig. (5). This fitted value of k_La is somewhat lower than the "ideal" value of $k_L \frac{6\varepsilon_G}{d_b}$ = 0.0075 s^{-1}. The lower value of the fitted k_La is primarily attributable to the departure from plug flow behavior of the gas phase in the disengagement section above the riser.

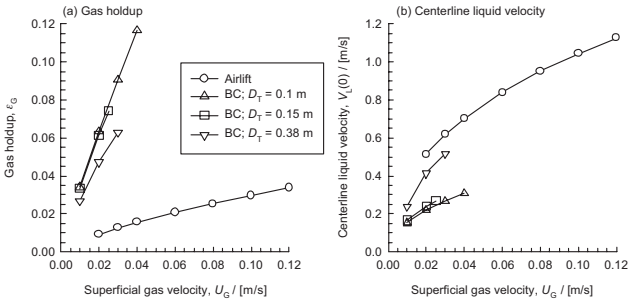

Figure 5. Comparison of: (a) gas holdup and (b) centreline liquid velocity, $V_L(0)$, for airlift reactor with bubble columns of 0.1, 0.15, and 0.38 m diameter. The superficial gas velocity, U_G, for the airlift is defined in terms of the riser cross-sectional area and the gas holdup is the global value in the system. Animations of bubble columns can be viewed on the web site: http://ct-cr4.chem.uva.nl/regimes/.

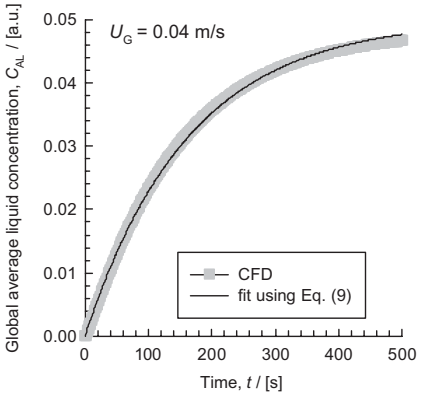

Figure 6. (a) Transient approach to the steady-state of the global average liquid concentration in the airlift. The fit to determine k_La, using Eq. (9) is shown as the continuous line. U_G = 0.04 m/s.

The fitted values of k_La for the airlift are compared in Fig. 7 (a) to the corresponding values obtained by CFD simulations of mass transfer in bubble columns of 0.1 and 0.38 m diameter.

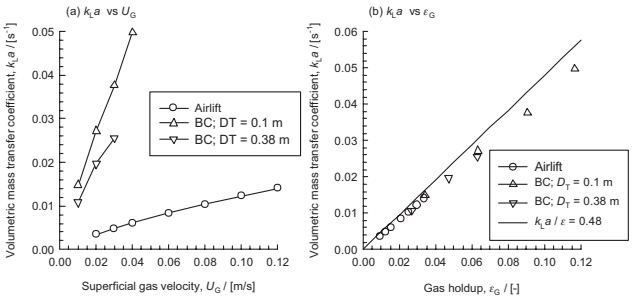

Figure 7. Volumetric mass transfer coefficients, k_La, obtained from fitting Eq. (9) for airlift and bubble columns of 0.1 and 0.38 m diameter. (b) Values of k_La plotted against the gas holdup, ε_G.

k_La values for the airlift configuration are considerably lower than the corresponding values for the bubble columns; this is due to the considerably lower gas holdup values. If the k_La values are plotted against the system gas holdups, it is seen that the values of the volumetric mass transfer coefficients for airlifts and bubble columns are comparable. From the data inputs in the simulations we should expect an "ideal" value $\frac{k_La}{\varepsilon_G} = 4 \times 10^{-4} \times \frac{6}{0.005} = 0.48$. It was noted that the k_La values are lower than this "ideal" value and the departures from ideality increase with increasing gas holdup, especially for the bubble column configurations. The reason for the departure from ideality is that with increasing gas holdup the gas flow in bubble columns, and to a lesser extent within the riser of the airlift configuration, deviates from plug flow.

4 Conclusions

In this paper CFD techniques for describing the hydrodynamics and mass transfer in airlift and bubble column reactors were discussed. The following major conclusions can be drawn from this study.

- The gas and liquid phases show virtual plug flow behavior within the riser of an airlift. This is in contrast with bubble columns where both gas and liquid phases deviate strongly from plug flow.
- When compared at the same superficial gas velocity, the liquid circulation is much stronger in airlifts than in bubble columns. This leads to a much lower gas holdup in airlifts. These higher circulation velocities can be advantageous in many practical applications.
- Due to the much lower slip between gas and liquid velocities in the riser of the airlift, homogeneous bubble flow can be maintained at much higher U_G values in airlifts than in bubble columns.
- The volumetric mass transfer coefficient, k_La, in airlifts is considerably lower than in bubble columns, this is a consequence of significantly lower gas holdup, ε_G.
- When airlift and bubble column reactors are compared at the same value of the system gas holdup, ε_G value, the volumetric mass transfer coefficient, k_La, is the same. This finding is of practical value for scale up purposes.

It can be concluded that CFD simulations can be a powerful tool for the modeling and design of airlift and bubble column reactors, especially in the context of describing the complex flow of the gas and liquid phases for different geometrical configurations.

Acknowledgement

The Netherlands Organization for Scientific Research (NWO) is gratefully acknowledged for providing financial assistance in the form of a "programmasubsidie" for the development of novel concepts in reactive separations technology.

Received: January 3, 2003 [CET 1796]

Symbols used

a	[m^2 m^{-3}]	interfacial area per unit volume of dispersion
C_D	[–]	drag coefficient
C_G	[arbitrary units]	gas phase concentration
C_L	[arbitrary units]	liquid phase concentration
C^*_L	[arbitrary units]	equilibrium liquid phase concentration
d_b	[m]	diameter of bubble
$Đ_k$	[m^2 s^{-1}]	diffusivity in phase k
D_T	[m]	column diameter
$Eö$	[–]	Eötvös number, $g(\rho_L - \rho_G)d_b^2/s$
F	[a.u. s^{-1}]	flux of mass tracer
g	[m s^{-2}]	gravitational acceleration
$\boldsymbol{g}$	[m s^{-2}]	gravitational vector
h	[m]	height above the distributor at bottom of reactor
H_T	[m]	total height of reactor
He	[–]	Henry coefficient
k_L	[m/s]	mass transfer coefficient in liquid phase
$\boldsymbol{M}$	[N/m^3]	interphase momentum exchange term
p	[Pa]	system pressure
r	[m]	radial coordinate
t	[s]	time
$\boldsymbol{u}$	[m/s]	velocity vector
U	[m s^{-1}]	superficial gas velocity in the riser
$V_L(r)$	[m s^{-1}]	radial distribution of liquid velocity
$V_L(0)$	[m s^{-1}]	centre-line liquid velocity

Greek symbols

ε	[–]	total gas hold-up
μ	[Pa s]	viscosity of fluid phase
ρ	[kg m^{-3}]	density of phase
σ	[N m^{-1}]	surface tension of liquid phase

Superscripts

*	equilibrium value

Subscripts

α	component in mass tracer experiment, dimensionless
G	referring to gas
in	referring to inlet to reactor
L	referring to liquid
out	referring to outlet of reactor
k,l	referring to phase k and l respectively
T	tower or column

References

[1] W. D. Deckwer, *Bubble Column Reactors*, John Wiley, New York **1992**.
[2] I. Bergault, M. V. Rajashekharam, R. V. Chaudhari, D. Schweich, H. Delmas, *Chem. Eng. Sci.* **1997**, *52*, 4033.
[3] C. Joly-Vuillemin, C. de Bellefon, H. Delmas, *Chem.Eng. Sci.* **1996**, *51*, 2149.
[4] H. Blenke, *Adv. Biochem. Eng.* **1979**, *13*, 121.
[5] M. Y. Chisti, *Airlift Bioreactors*, Elsevier Applied Science, London **1989**.
[6] A. E. Saez, M. A. Marquez, G. W. Roberts, R. G. Carbonell, *A.I.Ch.E.J.* **1998**, *44*, 1413.
[7] A. Cockx, A. Line, M. Roustan, Z. DoQuang, V. Lazarova, *Chem. Eng. Sci.* **1997**, *52*, 3787.
[8] J. J. Heijnen, J. Hols, R. G. J. M. van der Lans, H. L. M. van Leeuwen, A. Mulder, R. Weltevrede, *Chem. Eng. Sci.* **1997**, *52*, 2527.
[9] W. A. J. van Benthum, R. van der Lans, M. C. M. van Loosdrecht, J. J. Heijnen, *Chem. Eng. Sci.* **1999**, *54*, 3995.
[10] K. H. Choi, Y. Chisti, M. MooYoung, *Chem. Eng. J. Biochem. Eng. J.* **1996**, *62*, 223.
[11] C. Freitas, J. A. Teixeira, *Chem. Eng. J.* **2001**, *84*, 57.
[12] J. Korpijarvi, P. Oinas, J. Reunanen, *Chem. Eng. Sci.* **1999**, *54*, 2255.
[13] J. B. Joshi, *Chem. Eng. Sci.* **2001**, *56*, 5893.
[14] R. Krishna, M. I. Urseanu, J. M. van Baten, J. Ellenberger, *Chem. Eng. Sci.* **1999**, *54*, 4903.
[15] R. Krishna, J. M. van Baten, M. I. Urseanu, *Chem. Eng. Sci.* **2000**, *55*, 3275.
[16] R. Krishna, J. M. Van Baten, *Chem. Eng. Res. Des.* **2001**, *79*, 283.
[17] R. Krishna, J. M. van Baten, M. I. Urseanu, *Chem. Eng. Technol.* **2001**, *24*, 451.
[18] J. M. van Baten, R. Krishna, *Chem. Eng. Technol.* **2002**, *25*, 1081.
[19] J. M. van Baten, J. Ellenberger, R. Krishna, *Chem. Eng. Process.* **2003**, *42*, 733.
[20] J. Sanyal, S. Vasquez, S. Roy, M. P. Dudukovic, *Chem. Eng. Sci.* **1999**, *54*, 5071.
[21] A. Sokolichin, G. Eigenberger, *Chem. Eng. Sci.* **1999**, *54*, 2273.
[22] R. Clift, J. R. Grace, M. E. Weber, *Bubbles, Drops and Particles*, Academic Press, San Diego **1978**.
[23] C. M. Rhie, W. L. Chow, *A.I.A.A.J.* **1983**, *21*, 1525.
[24] J. van Doormal, G. D. Raithby, *Numer. Heat Transfer***1984**, *7*, 147.
[25] U. Jordan, A. Schumpe, *Chem. Eng. Sci.* **2001**, *56*, 6267.
[26] H. M. Letzel, J. C. Schouten, R. Krishna, C. M. van den Bleek, *Chem. Eng. Sci.* **1999**, *54*, 2237.

